39th IAHR WORLD CONGRESS GRANADA, SPAIN 2022 From Snow to Sea 19-24 June 2022

Proceedings of the 39th IAHR World Congress
19–24 June 2022, Granada, Spain
doi://10.3850/IAHR-39WC2521716X20221417

Sediment Scarcity: Modelling the Morphodynamics of Sandbanks When Sand Is Limited

Thomas J. van Veelen[1,2], Pieter C. Roos[1] and Suzanne J.M.H. Hulscher[1]

[1] University of Twente, Enschede, The Netherlands.
[2] Swansea University, Swansea, United Kingdom.
t.j.vanveelen@utwente.nl

Abstract

Sandbanks are large-scale dynamic bedforms of sandy sediment that are found in shallow seas. They may occur in areas where the sediment supply is limited such as on the Belgian Continental Shelf. These sandbanks serve important ecological and economic functions (e.g. sand extraction). However, our understanding of the long-term morphodynamics of tidal sandbanks under sediment-scarce conditions is limited due to a lack of process-based modelling support. Here, we study equilibrium cross-sections and the morphodynamic evolution towards an equilibrium by extending a process-based model to account for sediment scarcity. Our model includes a non-erodible layer, which limits sediment entrainment. The model results show that the presence of a non-erodible layer limits the amplitude of a sandbank and sharpens the crest in its equilibrium state. The bank width remains unaffected. Furthermore, our results show that sandbanks reach equilibria faster when a non-erodible layer is present. However, the rate of amplitude growth of a bank crest is unaffected for a long period after the non-erodible layer is exposed under the conditions in this study. Our results are valuable for identifying potential impacts of sand extractions in sandbank fields with limited sand available in the seabed.

Keywords: Tidal sandbanks; Sediment Scarcity; Morphodynamic modelling; Long-term evolution; Non-erodible Layers.

1. INTRODUCTION

Tidal sandbanks are large-scale marine bedforms observed at the bottom of shallow seas such as the North Sea and the East China Sea. They are tens of kilometres long, five to ten kilometres wide, and tens of metres high (de Swart & Yuan, 2019; Dyer and Huntley, 1999). Sandbanks typically lie with an orientation of 0-20 degrees anti-clockwise with respect to the tidal current on the Northern Hemisphere (Kenyon et al., 1981). They provide ecosystem services to marine flora and fauna (Atalah et al., 2013), and can be of interest for economic activities including wind farm construction, pipelines, and sand extraction (Fairley et al., 2016; Whitehouse et al., 2011; van Lancker et al., 2010).

Sandbanks are dynamic bedforms that evolve over centuries. Observations have revealed that sandbanks grow in height, change cross-sectional and planform shape, migrate, and may induce new bedforms (Mitchell et al., 2021; Dolphin, 2007; Reeve, 2001; Smith, 1988; Caston 1972). These observations have been supported by complex site-specific numerical models (Horrillo-Caraballo and Reeve, 2008; Deleu et al., 2004) and process-based models with idealized topographies (van Veelen et al., 2018; Yuan et al., 2017; Roos et al., 2004; Huthnance, 1982ab) Process-based models that focus on long time scales have also revealed that sandbanks, under steady environmental and tidal conditions, will eventually reach a static or dynamic equilibrium in which their cross-sectional growth is saturated (Yuan et al., 2017; Roos et al., 2004; Huthnance, 1982ab). The sandbanks may still exhibit migration or rhythmic changes in planform shape (Yuan et al., 2017).

It is yet unclear how the dynamics of sandbanks change when sediment is scarce. Sediment scarcity occurs when non-erodible layers are present just below the seafloor, as is the case on the Belgian and French continental shelves (Hademenos et al., 2019; Le Bot, 2001) and between the Norfolk banks (Caston, 1972). This restriction is often omitted in process-based models, which limits our understanding of the long-term dynamics of tidal sandbanks and the equilibrium cross-sections that they may attain. Huthnance (1982a) studied the impact of a non-erodible layer on equilibrium cross-sectional shapes under simplified hydrodynamics (block flow and no Coriolis effect) by restricting the final state sediment balance to the sandy part of the domain only. His analysis did not include the effects of the exposed non-erodible layers on sediment pick-up, settling and transport.

Therefore, we aim to understand how sediment scarcity affects the transient dynamics and equilibrium shapes of sandbanks via process-based modelling. We model sediment scarcity using a non-erodible layer,

which prevents sediment pick-up. In addition to equilibrium cross-sections, we also consider the evolution towards an equilibrium.

2. MODEL DESCRIPTION

We use the process-based numerical model by Roos et al. (2004) as the basis for our model. We introduce a non-erodible layer, and we change the sediment entrainment function such that it accounts for the availability of sand on the seabed.

2.1 Physics

Sandbanks are viewed as free instabilities of the seabed that are driven by tide-topography interactions (Huthnance, 1982ab). Our model considers tidal flow with different constituents (M_2,M_4), residual flow, Coriolis effects, bottom friction, wind-driven wave stirring, and suspended sediment. Sediment transport is restricted when a non-erodible layer is exposed in the troughs of the sandbank. We restrict ourselves to the dynamics along the cross-section of the sandbank, which reflects that the length of sandbanks is much larger than their width. Finally, all physics are considered depth-averaged, as the evolution of sandbanks is driven by horizontal circulation cells that are induced by tide-topography interactions (Hulscher et al., 1993).

2.2 Topography

We consider a sandbank in an offshore part of the sea, which is far away from coasts (Fig. 1). The seabed does not have a shelf slope and has a mean water depth H. Underneath a layer of uniform sediment, a non-erodible layer is located at a depth H_{rock}. No sediment can be picked up from this layer. The ambient tidal flow in this region is dominated by the semidiurnal M_2-tide with period T, maximum flow velocity U, and inclination θ with respect to the cross-bank direction.

We define a three-dimensional coordinate system with horizontal coordinate x in the cross-bank direction, y in along-bank direction, and z pointing upward in vertical direction. The water surface is located at $z = \zeta(x,t)$ and the topography of the bed is given by $z = -h(x, t_{mor})$. The topography varies in cross-sectional direction only and is a function of the morphological time coordinate $t_{mor} = T_{mor}t$ with morphological time scale T_{mor} and tidal time coordinate t. Furthermore, the width of the domain is chosen to match the length of the fastest growing mode from linear stability analysis (see e.g. Hulscher et al., 1993) and the boundaries of the domain are spatially periodic. Therefore, the topography effectively represents a field of infinitely long sandbanks (in y-direction) with a spacing that is consistent with the wave length of the fastest growing mode. The flow velocity within the domain is denoted by $\boldsymbol{u}(x,t) = (u,v)$.

The tidal forcing is represented by a tidal current, which is depth-averaged, spatially uniform and time-dependent. The contribution of the tidal range to the water depth is considered negligible. This assumption, which is known as the rigid lid assumption (Roos et al., 2004), is justified by the small value of the squared Froude Number for the tidal flow conditions considered here. $Fr^2 \approx 10^{-3}$ for the conditions considered in this study.

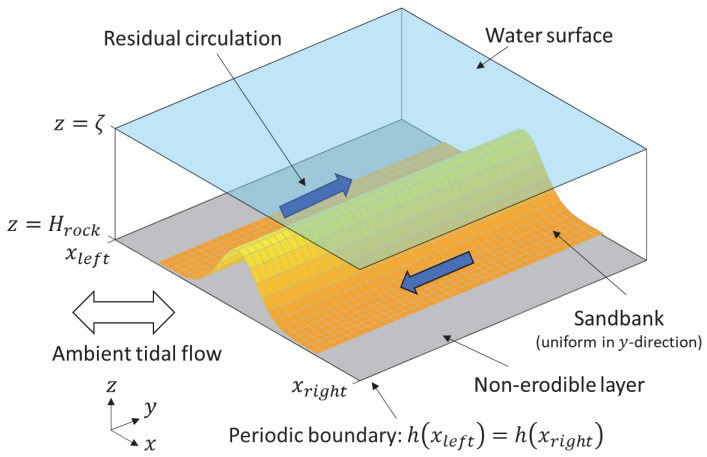

Figure 1. Sketch of model domain and topography. The yellow-coloured part of the domain shows a sandbank, and the grey plane denotes the non-erodible layer.

2.3 Governing Equations

The hydrodynamics are controlled by the nonlinear shallow water equations according to

$$\frac{\partial u}{\partial t} + u\frac{\partial u}{\partial x} - fv + \frac{ru}{h} = P_x - \frac{\partial \zeta}{\partial x}, \quad [1]$$

$$\frac{\partial v}{\partial t} + u\frac{\partial v}{\partial x} + fu + \frac{rv}{h} = P_y, \quad [2]$$

$$\frac{\partial hu}{\partial x} = 0. \quad [3]$$

Herein, f is the Coriolis parameter, r is a bottom friction coefficient, P_x is the x-component of the tidal forcing, and P_y is the y-component of the tidal forcing. Also, we have accounted for the fact that Froude number is small.

Sediment transport is controlled by the advection-diffusion equation (e.g., Schuttelaars and de Swart, 1996) given by

$$\frac{\partial c}{\partial t} + \frac{\partial cu}{\partial x} = \gamma(c_e - c), \quad [4]$$

with deposition coefficient γ, which controls the sediment transport mode, and entrainment concentration

$$c_e(x,t) = \mu\alpha_s\left(|\boldsymbol{u}|^2 + \frac{1}{2}u_w^2\right). \quad [5]$$

α_s is a proportionality coefficient and u_w is the depth-dependent stirring velocity driven by wind waves (Roos et al., 2004). As a new element, we introduce the entrainment limiter $\mu(h)$, which restricts sediment pick up from the non-erodible layer such that it represents sediment scarcity. The entrainment limiter is set at 0 at the non-erodible layer when $h = H_{rock}$ and it set a 1 above the non-erodible layer when $h < H_{rock} - \delta$. A buffer layer of thickness δ is located on top of the non-erodible layer. The buffer layer ensures that the entrainment concentration is continuous and improves numerical stability.

Finally, the bed evolution is computed using the Exner's equation

$$\frac{\partial h}{\partial t_{mor}} = \gamma\langle c_e - c\rangle + \lambda\frac{\partial}{\partial x}\left(\langle c_e\rangle\frac{\partial h}{\partial x}\right) \quad [6]$$

in which λ is a bed slope coefficient, and the brackets $\langle\cdot\rangle$ denote an average over a tidal cycle.

2.4 Solution Procedure

Our solution procedure is spectral in the temporal dimension and pseudo-spectral in the spatial dimension. The entrainment limiter μ and Eq. [5] are spatially solved in physical space. The other equations are expanded spatially and temporally into Fourier modes. In the simulations presented, the expansion is spatially truncated at 32 modes and temporally truncated at four modes. The morphodynamic time-stepping that follows from Eq. [6] is conducted using the semi-implicit scheme in Roos et al. (2004).

3. RESULTS

We have selected two sample cases from a range of simulations with the aim of illustrating how sediment scarcity affects sandbank morphodynamics. We compare the dynamics of a sandbank with a non-erodible layer (case A) against the dynamics of a sandbank with unlimited sand supply, i.e. without such a non-erodible layer (case B). Case A includes a non-erodible layer at a depth $H_{rock} = 35$ m and a buffer zone of 1 m via the entrainment limiter μ. Case B is equivalent to the simulations run in Roos et al. (2004) and does not employ an entrainment limiter. We simulate the evolution of a sandbank with an initial amplitude of 1.5 m until an equilibrium is reached. The flow and sediment conditions (Table 1) are set identical to the reference case without Coriolis and with suspended sediment transport in Roos et al. (2004) to enable comparison.

Table 1. Parameters used in model simulations.

PARAMETER	SYMBOL	VALUE	UNIT

Mean water depth	H	30	m
Depth non-erodible layer[a]	H_{rock}	35	m
Buffer layer thickness[a]	δ	1	m
Period of M_2-tidal cycle	T	4.47×10^5	s
Maximum tidal flow velocity	U	1	m s^{-1}
Inclination of the tidal flow	θ	27	deg
Coriolis parameter	f	0	s^{-1}
Bottom friction coefficient	r	2.5×10^{-3}	m s^{-1}
Deposition coefficient	γ	0.016	s^{-1}
Entrainment coefficient	α_s	4.0×10^{-5}	m^{-1} s^2
Wind stirring parameter	U_w	1	m s^{-1}
Bed slope coefficient	λ	2	m s^{-1}
Morphological time scale	T_{mor}	101	year
Squared Froude number	Fr^2	3.4×10^{-3}	-

3.1 Equilibrium Cross-section

The equilibrium shapes of the cross-sections of both cases show that the non-erodible layer leads to a lower crest height (Fig. 2). The crest of the sandbank attains a height of 22.4 m in Case A, which is 7.6 m below the water surface. The crest height in case B is 14.5m, which is 15.5 m below the water surface. Therefore, the presence of a non-erodible layer reduces the crest height by 7.9 m. The maximum trough depth of case A is 40.2 m below the surface or 10.2 m below mean water depth, whereas the trough depth of Case B is equal to the depth of the non-erodible layer at 35 m below the water surface.

An analysis of the shape of the equilibrium cross-section shows that sediment scarcity leads to sharper crests, but not to a change in bank width. The flat troughs in equilibrium cross-sections appear to be a natural phenomenon, as has been found in Roos et al. (2004). The presence of a uniform non-erodible layer also leads to flat troughs but at a shallower depth. The crest of case A is sinusoidal and sharper than that of case B. Due to the higher crest of case B, the diffusive effect of wind wave stirring is stronger, which flattens the crest shape. The width of both cases at mean water depth is comparable. This indicates that the slopes of the bank profile of case B are steeper.

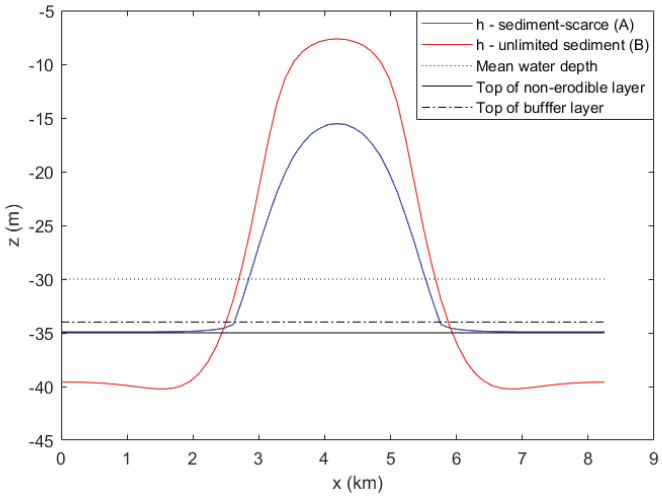

Figure 2. The equilibrium profiles of the sandbank with (case A, blue) and without (case B, red) a non-erodible layer. The mean water depth, the top of the non-erodible layer, and thickness of the buffer layer are also shown.

3.2 Evolution Towards Equilibrium

According to our model results, sandbanks subject to sediment scarcity may reach an equilibrium shape quicker than sandbanks with unlimited sediment available. The evolution towards the equilibrium of both cases is presented in Figure 3. Their evolution is identical as long as sufficient sediment is available. When the trough depth h_{trough} nears the non-erodible layer, the hard layer prevents further erosion of the trough in case A while the trough in case B continues to erodes until $t_{mor} = 10$ (≈ 1000 years). The crest height h_{crest} is not affected by the non-erodible layer until $t_{mor} = 7.5$, which is much later than when the non-erodible layer is exposed at

[a] Only used in case B.

$t_{mor} = 4$. This suggests that a larger area of the non-erodible layer must be exposed before the amplitude growth of the crest is affected by the scarcity of sediment. The growth in h_{crest} of case A quickly diminishes following the impact of the non-erodible layer at $t_{mor} = 7.5$, whereas h_{crest} continues to grow in case B until $t_{mor} = 14.5$. The timescale of evolution strongly depends on initial topography and morphodynamic conditions. Therefore, the main observations are that case A attains an equilibrium faster, and that the growth of the crest height is unaffected for centuries after the moment that the non-erodible layer is first exposed.

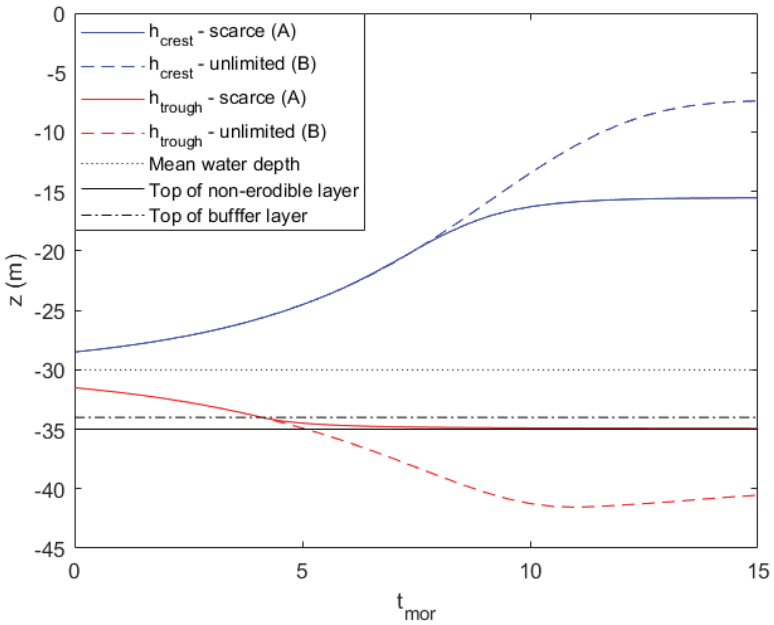

Figure 3. Evolution of the crest height h_{crest} and trough depth h_{trough} of the sandbanks with (case A, solid line) and without (case B, dashed line) a non-erodible layer. $t_{mor} = 1$ equates to 101 years.

4. CONCLUSIONS

Sediment scarcity has a significant impact on the cross-sectional shape of sandbanks in equilibrium and the transient evolution towards an equilibrium. Sandbanks that lie on top of a non-erodible layer have lower crests and shallower troughs in equilibrium conditions. The crests are also sharper when sediment is scarce. The width of the sandbank is unaffected by the presence of a non-erodible layer. As a result, the slopes of a sandbank with unlimited sand available are steeper than when sediment is scarce.

Sandbanks in sediment-scarce areas reach their equilibrium crest height and trough depth faster than when sediment is plentiful. Their evolution is identical when the trough depth is above the non-erodible layer. The erosion of the trough starts to differ immediately when the non-erodible layer is exposed. However, the crest height evolves the same for both banks long after the non-erodible layer is first exposed under the initial topography and morphodynamic conditions in this study. The crest height is limited for the sediment-scarce case after this period, while the bank with unlimited sediment availability continues to grow.

Our findings are relevant to the dynamics of sandbanks on continental shelf with limited sand such as the Belgian and French Continental Shelf. Sediment scarcity becomes especially relevant when sand extraction is envisioned in these areas. Our outcomes can help identifying potential impacts from sand extraction and contribute to the improvements in the design of sand extraction programs. As future steps, we plan to study the impact of sand extraction pits, and equilibria from topographies that vary in both horizontal directions.

5. REFERENCES

Atalah, J., Fitch, J., Coughlan, J., Chopelet, J., Coscia, I., and Farrell, E. (2013). Diversity of demersal and megafaunal assemblages inhabiting sandbanks of the Irish Sea. *Marine Biodiversity*, 43(2), 121–132. 10.1007/s12526-012-0139-y

Caston, V.N.D. (1972). Linear Sand Banks in the Southern North Sea. *Sedimentology*, 18(1–2), 63–78. 10.1111/j.1365-3091.1972.tb00003.x

de Swart, H.E. and Yuan, B. (2019). Dynamics of offshore tidal sand ridges, a review. *Environmental Fluid Mechanics*, 19(5), 1047–1071. 10.1007/s10652-018-9630-8

Deleu, S., Van Lancker, V., Van den Eynde, D., and Moerkerke, G. (2004). Morphodynamic evolution of the kink of an offshore tidal sandbank: The Westhinder Bank (Southern North Sea). *Continental Shelf Research*, 24(15), 1587–1610. 10.1016/j.csr.2004.07.001

Dolphin, T.J., Vincent, C.E., Coughlan, C., and Rees, J.M. (2007). Variability in Sandbank Behaviour at Decadal and Annual Time-Scales and Implications for Adjacent Beaches. *Journal of Coastal Research*, 731–737.

Dyer, K. R. and Huntley, D. A. (1999). The origin, classification and modelling of sand banks and ridges. *Continental Shelf Research*, 19(10), 1285–1330. 10.1016/S0278-4343(99)00028-X

Fairley, I., Masters, I., & Karunarathna, H. (2016). Numerical modelling of storm and surge events on offshore sandbanks. *Marine Geology*, 371, 106–119. 10.1016/j.margeo.2015.11.007

Hademenos, V., Stafleu, J., Missiaen, T., Kint, L., & Lancker, V.R.M.V. (2019). 3D subsurface characterisation of the Belgian Continental Shelf: A new voxel modelling approach. *Netherlands Journal of Geosciences*, 98. 10.1017/njg.2018.18

Horrillo-Caraballo, J.M., and Reeve, D.E. (2008). Morphodynamic behaviour of a nearshore sandbank system: The Great Yarmouth Sandbanks, U.K. *Marine Geology*, 254(1), 91–106. 10.1016/j.margeo.2008.05.014

Hulscher, S.J.M.H., de Swart, H.E., and de Vriend, H.J. (1993). The generation of offshore tidal sand banks and sand waves. *Continental Shelf Research*, 13(11), 1183–1204. 10.1016/0278-4343(93)90048-3

Huthnance, J.M. (1982a). On one mechanism forming linear sand banks. *Estuarine, Coastal and Shelf Science*, 14(1), 79–99. 10.1016/S0302-3524(82)80068-6

Huthnance, J.M. (1982b). On the formation of sand banks of finite extent. *Estuarine, Coastal and Shelf Science*, 15(3), 277–299. 10.1016/0272-7714(82)90064-6

Kenyon, N.H., Belderson, R.H., Stride, A.H., and Johnson, M.A. (1981). Offshore Tidal Sand-Banks as Indicators of Net Sand Transport and as Potential Deposits. In *Holocene Marine Sedimentation in the North Sea Basin*. John Wiley & Sons, Ltd, 257–268. 10.1002/9781444303759.ch20

Le Bot, S. (2001). *Morphodynamique de dunes sous-marines sous influence des marées et des tempêtes: Processus hydro-sédimentaires et enregistrement : exemple du Pas-de-Calais*. University of Lille, pp. 311.

Mitchell, N.C., Jerrett, R., and Langman, R. (2021). Dynamics and stratigraphy of a tidal sand ridge in the Bristol Channel (Nash Sands banner bank) from repeated high-resolution multibeam echo-sounder surveys. *Sedimentology*. 10.1111/sed.12935

Reeve, D.E., Li, B., and Thurston, N. (2001). Eigenfunction Analysis of Decadal Fluctuations in Sandbank Morphology at Gt Yarmouth. *Journal of Coastal Research*, 17(2), 371–382.

Roos, P.C., Hulscher, S.J.M.H., Knaapen, M.A.F., and Damme, R.M.J.V. (2004). The cross-sectional shape of tidal sandbanks: Modeling and observations. *Journal of Geophysical Research: Earth Surface*, 109(F2). 10.1029/2003JF000070

Schuttelaars, H.M. and Swart, H.E. de (1996). An idealized long-term morphodynamic model of a tidal embayment. *European Journal of Mechanics*, 15, 55–80.

Smith, D.B. (1988). Stability of an offset kink in the North Hinder Bank. *Tide-Influenced Sedimentary Environments and Facies*, Ed. P. de Boer, A. van Gelder, and S.-D. Nio, D. Reidel Publishing Company, Dordrecht, The Netherlands, 65-78. 10.1007/978-94-015-7762-5_6

Van Lancker, V.R.M., Bonne, W.M.I., Garel, E., Degrendele, K., Roche, M., Van den Eynde, D., Bellec, V.K., Brière, C., Collins, M.B., and Velegrakis, A.F. (2010). Recommendations for the sustainable exploitation of tidal sandbanks. *Journal of Coastal Research*, 151–164.

Whitehouse, R.J.S., Harris, J.M., Sutherland, J., and Rees, J. (2011). The nature of scour development and scour protection at offshore windfarm foundations. *Marine Pollution Bulletin*, 62(1), 73–88. 10.1016/j.marpolbul.2010.09.007

Yuan, B., de Swart, H.E., and Panadès, C. (2017). Modeling the finite-height behavior of offshore tidal sand ridges, a sensitivity study. *Continental Shelf Research*, 137, 72–83. 10.1016/j.csr.2017.02.007

